RNAi screening for fat regulatory genes with SRS microscopy

Meng C Wang[1,2,6], Wei Min[3,5,6], Christian W Freudiger[3,4], Gary Ruvkun[2] & X Sunney Xie[3]

Identification of genes regulating fat accumulation is important for basic and medical research; genetic screening for those genes in *Caenorhabditis elegans*, a widely used model organism, requires *in vivo* quantification of lipids. We demonstrated RNA interference screening based on quantitative imaging of lipids with label-free stimulated Raman scattering (SRS) microscopy, which overcomes major limitations of coherent anti-Stokes Raman scattering microscopy. Our screening yielded eight new genetic regulators of fat storage.

Obesity has reached epidemic proportions globally and is a major risk factor for chronic diseases, such as type-2 diabetes, cardiovascular diseases and hypertension. To better prevent and treat obesity and its associated metabolic disorders, it is necessary to understand the regulatory mechanisms of fat accumulation and distribution at both cellular and organism levels. Genomic screening for fat-storage modulators has been carried out in several single-cell or multicellular organisms, including *Saccharomyces cerevisiae*, *Caenorhabditis elegans, Drosophila melanogaster* and *D. melanogaster* S2 cells[1–5]. *C. elegans* has proven to be a promising multicellular organism for high-throughput genomic studies partly because of its small size, well-developed genetic tools and ease of handling.

Lipid analysis in *C. elegans* has been performed by traditional biochemical approaches, fixation and staining, fluorescence imaging of live worms through vital dye feeding and most recently via label-free coherent anti-Stokes Raman scattering (CARS) microscopy[6]. However, all of these approaches have serious limitations. Biochemical assays require extraction of lipids from more than 5×10^3 worms and subsequent time-consuming chromatography analysis[6], which cannot be easily carried out on the genomic scale. The organic solvents used in the fixation protocol often disrupt and interfere with the structure of lipid-storage compartments. Analysis after feeding with vital dyes, such as Nile Red and boron-dipyrromethene (BODIPY), is rather indirect and is complicated by unpredictable dye-incorporation efficiency and the lack of a linear relationship between the observed signal and the actual lipid quantity. Several studies have revealed inaccuracy

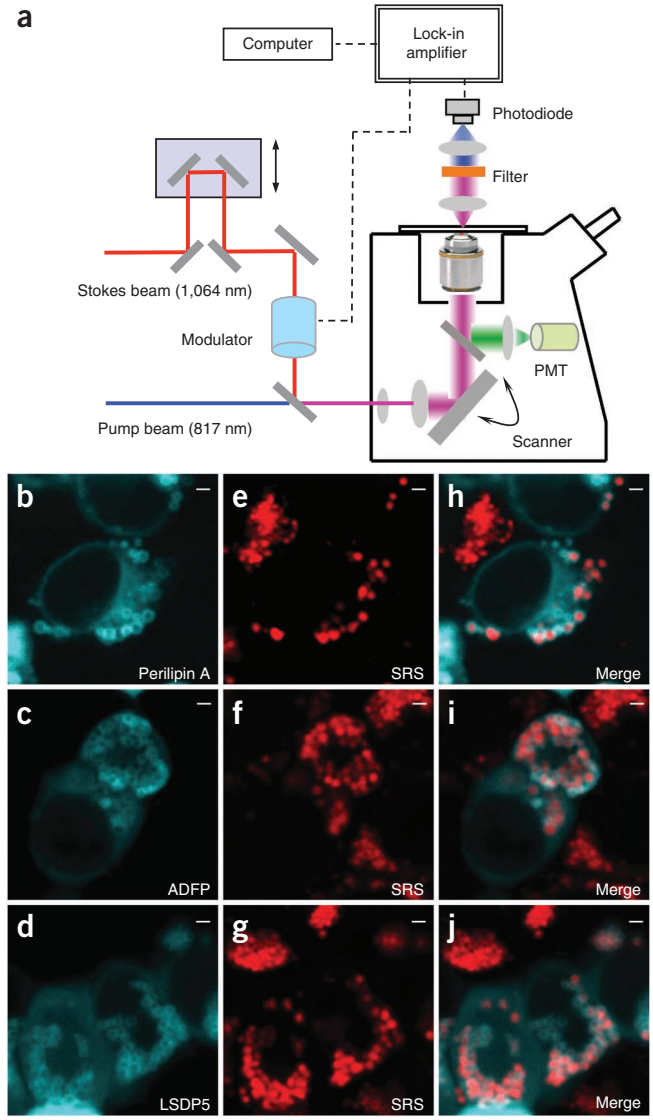

Figure 1 | Visualization of cellular fat storage in lipid droplets using SRS microscopy. (**a**) Experimental scheme of label-free SRS microscopy for *in vivo* lipid imaging. PMT, photomultipier tube. (**b**–**d**) YFP fluorescence images (**b**–**d**), SRS signals (**e**–**g**) and merged images (**h**–**j**) of HEK 293 cells expressing YFP-tagged perilipin A (**b**,**e**,**h**), ADFP (**c**,**f**,**i**) and LSDP5 (**d**,**g**,**j**). Scale bars, 1 μm.

[1]Department of Molecular and Human Genetics and Huffington Center on Aging, Baylor College of Medicine, Houston, Texas, USA. [2]Department of Molecular Biology, Massachusetts General Hospital, and Department of Genetics, Harvard Medical School, Boston, Massachusetts, USA. [3]Department of Chemistry and Chemical Biology, Harvard University, Cambridge, Massachusetts, USA. [4]Department of Physics, Harvard University, Cambridge, Massachusetts, USA. [5]Present address: Department of Chemistry, Columbia University, New York, New York, USA. [6]These authors contributed equally to this work. Correspondence should be addressed to X.S.X. (xie@chemistry.harvard.edu), M.C.W. (wmeng@bcm.tmc.edu) or W.M. (wm2256@columbia.edu).

RECEIVED 22 SEPTEMBER 2010; ACCEPTED 17 DECEMBER 2010; PUBLISHED ONLINE 16 JANUARY 2011; DOI:10.1038/NMETH.1556

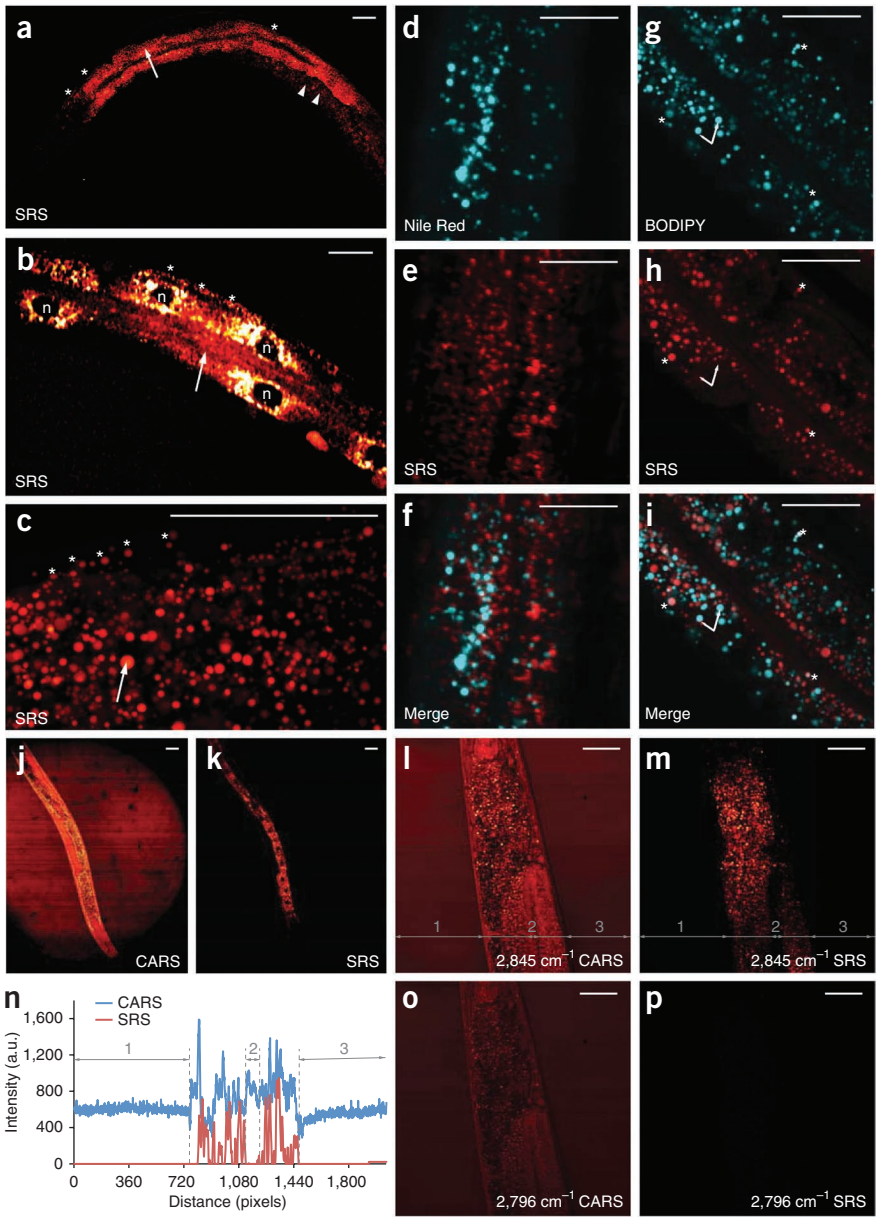

Figure 2 | Imaging fat accumulation and distribution in *C. elegans* by SRS microscopy. (**a**,**b**) SRS signals revealed fat storage in intestine (arrow), hypodermis (asterisk), early embryos in the uterus (arrowhead) and cellular nuclei (labeled with "n"). (**c**) Subcelluar fat accumulation in a pool of droplets observed by SRS microscopy. (**d**–**f**) Two-photon–excited fluorescence from Nile Red staining (**d**), SRS signals (**e**) and the overlaid images of these two signals (**f**). (**g**–**i**) BODIPY staining of two distinct groups of subcellular organelles with weaker (asterisk) and stronger (arrow) fluorescence signals (**g**), (SRS) image of the same organelles (**h**), and overlap of BODIPY and SARS signals (**i**). (**j**,**k**) CARS images showing strong signals in the intestinal cell nuclei owing to nonresonant background (**j**) and SRS image of the same worm with dark nuclei in the intestinal cells (**k**). (**l**–**p**) CARS and SRS images of the same worm taken at a Raman shift of 2,845 cm^{-1} resonant with CH_2 stretching mode (**l**,**m**) and a Raman shift of 2,796 cm^{-1} off-resonant (**o**,**p**). Cross-section profiles of the regions marked by gray lines in **l** and **m** are shown in **n**. Scale bars, 50 μm.

of vital-dye staining methods in live worms[6]. CARS microscopy is a label-free imaging technique, but CARS signals exhibit nonresonant background that limits detection sensitivity and creates imaging artifacts[7]. In addition, CARS signals have a complicated nonlinear relationship to analyte concentration[7].

Stimulated Raman scattering (SRS) microscopy can be used to excite and detect the CH_2 stretching vibration of fatty acid chains, which enables label-free three-dimensional lipid visualization with high sensitivity and specificity[7]. In brief, two ultrafast laser pulse trains, pump and Stokes, were spatially and temporally overlapped and coupled into a laser-scanning microscope (**Fig. 1a**). The Stokes beam had a fixed wavelength at 1,064 nm and was intensity modulated at 10 MHz. To image lipids, the pump beam was tuned into 817 nm, with the energy difference between the pump and the Stokes beams resonant with the vibrational energy of the CH_2 stretching mode. At the laser focus, a portion of energy was transferred from the pump pulse (intensity loss) to the Stokes pulse (intensity gain), owing to the nonlinear Raman interaction with the CH_2 vibrational mode. After passing through the sample, the forward-going pump beam was selectively transmitted through a filter and focused onto a silicon (Si) photodiode. The output current of the photodiode was fed into a lock-in amplifier to extract the stimulated Raman loss (SRL) signal of the pump beam precisely at 10 MHz. The SRL output from the amplifier was next fed back into the microscope and provided images of lipid in the sample. The SRL signal intensity was proportional to the concentration of targeted species.

We at first examined SRS lipid signals in living HEK 293 cells and confirmed their origin from cellular lipid droplets. The PAT family proteins, perilipin A, adipose differentiation-related protein (ADFP) and LSDP5 are well-conserved lipid droplet–associated proteins that localize to the droplet surface[8] (**Fig. 1b–d**). We found that cellular SRS signals corresponded exclusively to lipid droplets that were highlighted by the YFP-tagged PAT proteins (**Fig. 1b–j**) or probed by BODIPY fluorescence (**Supplementary Fig. 1**). Thus, using SRS microscopy we indeed detected cellular fat storage in lipid droplets specifically.

We next applied SRS microscopy to image fat storage in live worms (**Fig. 2**). At lower magnification, we observed fat distribution in the entire organism. The SRS signal had the highest intensity in the intestine, suggesting it was the primary site for fat storage (**Fig. 2a**). We detected weaker signals in the hypodermis, the oocyte and early stage embryos in the uterus (**Fig. 2a**,**b**). Inside a cell, the nucleus is known to be the organelle with the lowest fat accumulation. Consistently, the SRS signal was absent in the intestinal-cell nucleus (**Fig. 2b**), confirming a high

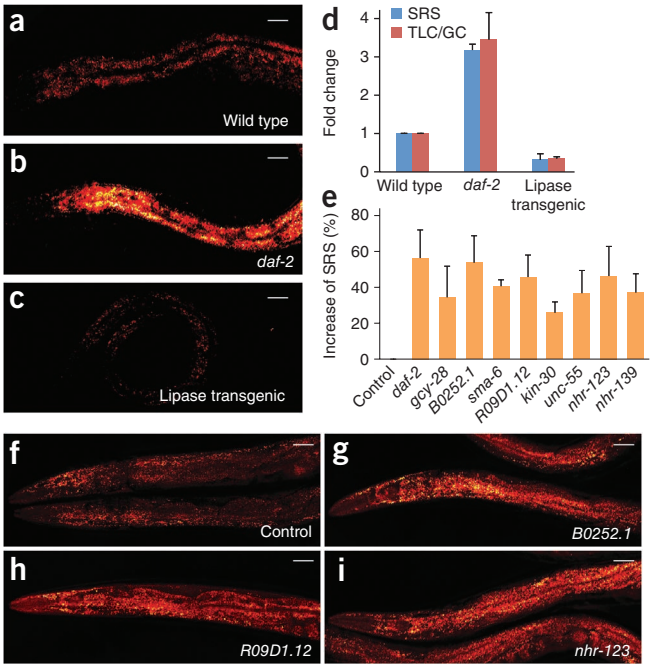

Figure 3 | RNAi screening of new fat storage regulatory genes based on *in vivo* lipid quantification using label-free SRS microscopy. (**a**–**c**) Fat was visualized by SRS in the wild-type worm (**a**), the *daf-2(e1370)* mutant (**b**) and the transgenic worm intestinally overexpressing the *K04A8.5* lipase (**c**) under same imaging conditions. (**d**) Quantification of fat content by SRS (n = 5 worms) and thin-layer chromatography–gas chromatography (TLC/GC) ($n = 5 \times 10^3$ worms). (**e**) SRS signal increase compared to the control for genes that resulted in a fat content increase of more than 25% when inactivated by RNAi ($P < 0.0001$, n = 5 worms). Control, worms fed with bacteria containing empty vectors. All the experiments were performed twice independently. Results from one experiment are shown. (**f**) Normal fat accumulation as observed in the RNAi hypersensitive strain, *nre-1(hd20)lin-15b(hd126)*, fed with empty vector–containing bacteria (control). (**g**–**i**) SRS images of three candidate worms. Scale bars, 50 μm. Error bars, s.d.

selectivity of the SRS method for lipid imaging *in vivo*. The spatial resolution of SRS is similar to that of two-photon–excited fluorescence microscopy[7]. We detected fat accumulation in subcellular compartments using SRS microscopy at higher magnification (**Fig. 2c**).

Nile Red fluorescence in live worms fed with this vital dye emits most intensely from gut granules[6]. We found that Nile Red fluorescence in the intestine was largely nonoverlapping with SRS signals (**Fig. 2d**–**f**), suggesting that gut granules are normally not fat storage compartments. BODIPY lipid probes were more reliable vital dyes than Nile Red in most systems such as cell culture (**Supplementary Fig. 1**). However, when fed to live worms, BODIPY fluoresced in both gut granules and lipid droplets (**Fig. 2g**–**i**). The latter signals localized together with SRS lipid signals, but their intensities were much weaker than those of nonlipid fluorescence from gut granules (**Fig. 2g**–**i**). Thus, lipid quantification based on BODIPY staining in live worms will be misleading because the brightest fluorescence was not lipid related.

Label-free CARS microscopy overcomes the above complications associated with fluorescent dye staining[9,10]. However, when compared to SRS imaging on the same worm, the CARS signals had much higher background from structures unrelated to lipids (**Fig. 2j**–**m** and **Supplementary Fig. 2**), which caused difficulties in image interpretation and lipid quantification. For example, the germline region containing undifferentiated germ cells had little lipid accumulation, which was therefore absent of SRS signals (**Fig. 2m**,**n**) but had high background in CARS microscopy (**Fig. 2l**,**n**). Unlike the CARS signal, the SRS signal was linear to the substance concentration and did not exhibit a nonresonant background (**Fig. 2m**,**n**,**p**), which will allow straightforward quantification of fat content via *in vivo* imaging.

To confirm the quantification ability of SRS imaging for *in vivo* application, we compared wild-type worms, an insulin receptor mutant, *daf-2(e1370)* that is known to have increased fat storage[5] and worms overexpressing a lipase gene that have reduced fat content[11] (**Fig. 3a**–**d**). We imaged 2-d-old young adults and calculated the mean SRS signal intensity. Compared to the wild type, the *daf-2(e1370)* mutants had 3.2-fold greater fat storage (**Fig. 3b**,**d**), and the lipase transgenic worms had 31% fat content (**Fig. 3c**,**d**). In parallel, we separated lipids extracted from ~5×10^3 worms using thin-layer chromatography, *trans*-esterized to fatty acid methyl esters and quantified by gas chromatography. The *in vivo* SRS and the *in vitro* thin-layer chromatography–gas chromatography quantification provided similar results for each of the three phenotypes (**Fig. 3d**), suggesting SRS imaging is a reliable and quantitative method for assaying fat phenotypes of *C. elegans*. In contrast, the quantification based on CARS signals did not reveal a difference in fat storage between the wild type and the mutants (**Supplementary Fig. 3**). Although there are sophisticated techniques for quantitative CARS imaging, the background-free chemical contrast of SRS microscopy offers pronounced advantage particularly for large-scale genomic screening.

We next performed RNAi screening using this label-free SRS method, which allowed us to search for fat storage regulatory genes under physiological conditions. Membrane receptors and nuclear receptors are crucial in transducing signaling of growth factors, cytokine and hormones, and there is precedent for their involvement in the regulation of fat storage, such as insulin receptor, leptin receptor and PPAR gamma[12]. To identify additional fat storage regulatory genes, we picked RNAi clones that target 36 cell-surface receptor genes and 236 nuclear hormone receptor genes in *C. elegans*. To enhance RNAi, especially in neurons, we used the RNAi hypersensitive strain, *nre-1(hd20)lin-15b(hd126)*[13] to knock down these genes. We screened 2-d-old young adults for their fat content in 8-well imaging chambers using SRS microscopy. Of the 272 genes we screened for, we discovered 9 genes whose inactivation increased fat content more than 25% (**Fig. 3e**–**i** and **Supplementary Fig. 4**).

All identified genes, except the insulin/IGF-1 receptor, *daf-2*, were new regulators of fat storage whose roles in fat metabolism are largely unknown. Each identified gene has a human homolog and is broadly expressed in multiple tissues including neurons (**Supplementary Table 1**). *gcy-28* is a worm homolog of human natriuretic peptide receptor. In the human, natriuretic peptides are cardiac hormones, which can induce lipid mobilization and oxidation in adipose tissue[14]. Consistently, we found that *gcy-28* inactivation increased worm fat content by 34% (**Fig. 3e** and **Supplementary Fig. 4**). We predict that other newly identified genes might also regulate mammalian fat metabolism.

Interfaced with RNAi, SRS microscopy allows discovery of genes regulating fat metabolism under physiological conditions of worms. The label-free feature greatly simplifies sample preparation and is well suited for cell tracking in model organisms[15] and for high-throughput screening as we demonstrated here. Using this method, a genome-wide search of new fat storage regulatory genes is under way.

METHODS

Methods and any associated references are available in the online version of the paper at http://www.nature.com/naturemethods/.

Note: Supplementary information is available on the Nature Methods website.

ACKNOWLEDGMENTS

We thank members of the H. Hutter laboratory (Simon Fraser University) for providing the *nre-1(hd20)lin-15b(hd126)* strain, members of the C. Sztalryd lab (University of Maryland School of Medicine) for providing perilipin A, ADFP and LSDP5 plasmids, J. Melo and Y. Hao for helping with the membrane receptor RNAi library, A. Soukas and H. Mak for helping with the nuclear hormone receptor RNAi library, Z. Shi for helping with RNAi clone sequencing, X. Zhang and B. Saar for helping on imaging instrumentation, P. Iakova and A. Folick for helping with mammalian cell transfection and C. He and J. Kang for gas chromatography analysis. This work was supported by US National Institutes of Health grants AG034988 (M.C.W.) and EB010244 (X.S.X.) and a predoctoral fellowship from Boehringer Ingelheim Fonds (C.W.F.).

AUTHOR CONTRIBUTIONS

M.C.W., W.M. and X.S.X. conceived the study; M.C.W. and W.M. designed the experiments; M.C.W., W.M. and C.W.F. performed the experiments; M.C.W. analyzed the data; M.C.W., W.M., G.R. and X.S.X. wrote the manuscript.

COMPETING FINANCIAL INTERESTS

The authors declare no competing financial interests.

Published online at http://www.nature.com/naturemethods/.
Reprints and permissions information is available online at http://npg.nature.com/reprintsandpermissions/.

1. Fei, W. *et al. J. Cell Biol.* **180**, 473–482 (2008).
2. Guo, Y. *et al. Nature* **453**, 657–661 (2008).
3. Pospisilik, J.A. *et al. Cell* **140**, 148–160 (2010).
4. Szymanski, K.M. *et al. Proc. Natl. Acad. Sci. USA* **104**, 20890–20895 (2007).
5. Ashrafi, K. *et al. Nature* **421**, 268–272 (2003).
6. Watts, J.L. *Trends Endocrinol. Metab.* **20**, 58–65 (2009).
7. Freudiger, C.W. *et al. Science* **322**, 1857–1861 (2008).
8. Wang, H. *et al. J. Biol. Chem.* **284**, 32116–32125 (2009).
9. Hellerer, T. *et al. Proc. Natl. Acad. Sci. USA* **104**, 14658–14663 (2007).
10. Yen, K. *et al. PLoS ONE* **5**, e12810 (2010).
11. Wang, M.C., O'Rourke, E.J. & Ruvkun, G. *Science* **322**, 957–960 (2008).
12. Gesta, S., Tseng, Y.H. & Kahn, C.R. *Cell* **131**, 242–256 (2007).
13. Schmitz, C., Kinge, P. & Hutter, H. *Proc. Natl. Acad. Sci. USA* **104**, 834–839 (2007).
14. Lafontan, M. *et al. Trends Endocrinol. Metab.* **19**, 130–137 (2008).
15. Olivier, N. *et al. Science* **329**, 967–971 (2010).

ONLINE METHODS

Apparatus. The apparatus of SRS microscopy setup is similar to what has been described in reference 7.

Laser arrangement. A Nd:YVO_4 pump laser (picoTRAIN, High-Q Laser Production) provided an output pulse train at 1,064 nm with 7-ps pulse width and 76-MHz repetition rate. This served as the Stokes beam. The frequency-doubled output at 532 nm was used to synchronously seed an optical parametric oscillator (OPO) (Levante Emerald, APE) to produce a mode-locked pulse train (the idler beam of the OPO is blocked with an interferometric filter) from 700 nm to 900 nm. This served as the pump beam. The wavelength tuning of the OPO involved a coarse temperature tuning of a noncritically phase-matched lithium triborate (LBO) crystal and a fine angle tuning of a stacked Lyot filter. The intensity of the 1,064-nm Stokes beam was modulated by an acousto-optical modulator (AOM) (model 3080-122, Crystal Technology) at 10 MHz driven by a square-wave-function generator. Modulation depth was more than 80% when the Stokes beam was gently focused inside the AOM crystal. The pump beam was spatially overlapped with the Stokes beam with a dichroic mirror (1064 DCRB, Chroma Technology). The temporal overlap between pump and Stokes pulse trains was ensured with a mechanical delay stage and measured with an autocorrelator (PulseCheck, APE).

Microscopy arrangement. Pump and Stokes beams were coupled into a modified laser scanning upright microscope (BX61WI/FV300, Olympus) optimized for near-infrared throughput. The beam size was matched to fill the back aperture of objectives. For fast whole-worm lipid screening, a 20× air objective (UPlanAPO, 0.75 numerical aperture (NA), Olympus) was used as an excitation lens. For high-resolution imaging, a 60× water objective (UPlanAPO/IR, 1.2 NA, Olympus) was then used. The forward-going pump and Stokes beams after passing through the sample were collected in transmission with a high-NA condenser lens (oil immersion, 1.4 NA, Nikon), which was aligned following Kohler illumination. A telescope was then used to image the scanning mirrors onto a large-area (10 mm × 10 mm) Si photodiode (FDS1010, Thorlabs) to avoid (for example, descan) beam motion during laser scanning. The photodiode was reversed bias by 60 V from a direct current power supply to increase the saturation threshold. A high optical density (OD) bandpass filter (890/220 CARS, Chroma Technology) was used to block the Stokes beam completely and transmit the pump beam only.

SRS imaging. The output current of the photodiode was electronically prefiltered by a bandpass filter (BBP-10.7, Mini Circuits) to suppress both the 76-MHz laser pulsing and the low-frequency contribution owing to laser scanning across the scattering sample. It was then fed into a radio frequency lock-in amplifier (SR844, Stanford Research Systems) terminated with 50 Ω to demodulate the stimulated Raman loss signal of the pump beam. The *x* output (in-phase component) of the lock-in amplifier was fed back into the analog-to-digital (A/D) converter of the microscope input. The time constant was set for 10 μs (with no additional filter applied in lock-in amplifier). For imaging, 512 pixels by 512 pixels were acquired for one frame with 100-μs pixel dwell time.

CARS imaging. CARS signal was collected by the same excitation objective in the backward direction and directed onto a red-sensitive photomultiplier tube (PMT) (R3896, Hamamatsu) mounted at a nondescanned epi position. In front of the CARS PMT, a combination of a short pass filter and a bandpass filter (ET750sp-2p8, H660/20, Chroma Technology) was used to block the pump and Stokes beams and any induced two-photon fluorescence.

Fluorescence imaging. Two-photon excited fluorescence images of Nile Red– or BODIPY-stained *C. elegans*, and PAT protein–transfected or BODIPY-stained HEK 293 cells were collected in the same setup used for the SRS microscopy measurements by using only the 1,064-nm Stokes beam. The two-photon fluorescence emission was detected in the backward direction by a PMT (R3896, Hamamatsu) equipped with a filter (ET750sp-2p8, Chroma Technology) to block the Stokes beam and another filter for fluorescence imaging (H580/30 (Nile Red), 550/30 (YFP) or 510/20 (BODIPY), Chroma Technology). The fluorescence stack was first recorded (with the 817-nm beam blocked), followed by the corresponding SRS stack of the same specimen by unblocking the 817-nm beam.

Strains. *C. elegans* N2 Bristol was used as the wild-type strain. We have also used the following *C. elegans* strains and mutant alleles: *daf-2(e1370)III*, *nre-1(hd20)lin-15b(hd126)X* and *mgIs[ges-1p::K04A8.5::gfp]*.

RNAi feeding and screening. RNAi bacteria were cultured 12–14 h in LB with 50 μg ml^{-1} carbenicillin and seeded onto 12-well agar plates containing 5 mM isopropylthiogalactoside (IPTG). The plates were allowed to dry in a laminar flow hood and incubated at room temperature (22 °C) overnight to induce dsRNA expression. Approximately 20–30 synchronized worms at the first larval stage were placed into each well of the plates containing bacteria expressing dsRNA targeting each worm gene. The worms were kept at 20 °C for 4 d until day-2 adulthood. Adult worms were washed off plates using M9 buffer with 0.1% sodium azide and transferred into 8-well chambered microscope cover glasses. Worms were imaged to determine fat storage phenotype and screened by the SRS microscopy system.

SRS and CARS signal quantification. For each genotype, ~15 anesthetized worms were mounted on a microscope slide with a centered agar pad. Five images were randomly captured as described above for SRS and CARS imaging. The 20× air objective has larger depth of view, and adult worms were ~90 μm in diameter and further flattened when mounted onto slides. Thus projection images were captured instead of taking three-dimensional sections, which greatly accelerated the analysis process. Using Image, mean intensity of SRS or CARS signals in the worms' anterior was calculated and subtracted from the mean intensity in the signal-free area. The average of five images was presented.

Thin-layer chromatography–gas chromatography quantification. About 5×10^3 adult worms were washed off large regular worm plates using M9 buffer, filtered through 35-μm nylon mesh to remove eggs and L1 larvae, and placed onto empty plates for 20 min at room temperature to clean up undigested bacteria in the gut. The worms were collected into 400 μl of PBS and homogenized through grinding followed by sonication. We used 50 μl of homogenate to measure protein concentration, and the other

250 µl of samples were used for lipid extraction with 5 ml of chloroform:methanol (1:1) overnight at 4 °C. The extract was washed with 1 ml of 0.15 M KCl and lipids were recovered in the chloroform phase and dried under nitrogen. We added 1 µg of tritridecanoin (C13:0 triglyceride, Nu-Chek Prep) as internal standard. Different lipid classes were separated by thin-layer chromatography on silica gel plates, and the triglyceride fraction was recovered for fatty acid *trans*-esterization. The resulting fatty acid methyl esters were analyzed by gas chromatography, and their levels were normalized to internal standard (C13:0). The triglyceride concentration was calculated based on fatty acid methyl ester amounts and further normalized to protein quantity.

Cell culture. HEK 293 cells (293 cells) were grown in Dulbecco's Modified Eagle medium (DMEM) supplemented with 10% FCS, 2 mmol l^{-1} L-glutamine, 100 units ml^{-1} penicillin and 100 µg ml^{-1} streptomycin at 37 °C with 5% CO_2 and 95% humidity. The constructs peri-YFP, LSDP5-YFP and ADFP-YFP were transfected into the 293 cells using FuGene 6 transfection reagent (Roche) according to the manufacturer's instructions. Six hours after transfection, the cells were incubated with growth medium supplemented with 400 µM oleic acid complexed with BSA. The cell images were captured in DMEM without phenol red using a 60× water objective after 12-h fatty acid supplement. For BODIPY staining, the cells were incubated with growth medium containing 2 µg ml^{-1} BODIPY for 60 min and imaged in DMEM without phenol red using a 60× water objective.

doi:10.1038/nmeth.1556